Microscopic approach for intersubband-based thermophotovoltaic structures in the terahertz and mid-infrared

PEREIRA, Mauro <http://orcid.org/0000-0002-2276-2095>

Editorially Accepted for Publication at JOSA B

Microscopic Approach for Intersubband-Based Thermophotovoltaic Structures in the THz and Mid Infrared

M.F. Pereira Jr[1]

[1]*Materials and Engineering Research Institute, Sheffield Hallam University, S1 1WB, Sheffield, United Kingdom*

email: M.Pereira@shu.ac.uk

This paper describes microscopic calculations of photocurrent generation spectra due to intersubband transitions in semiconductor heterostructures that can extract energy from photons in the THz and Mid Infrared Ranges. As expected in the mid infrared the interconduction conduction band transitions dominate the photocurrent. However, the numerical results presented here show that in the far infrared there is a range in which valence-band-based transitions dominate the photocurrent and these can be sustained under perpendicular incidence. This would lead to devices that do not need prisms and couplers in contrast with conduction-band based intersubband absorbers. Examples for different quantum well structures and different thermal source temperatures are compared and contrasted numerically. It is further demonstrated that many body effects, so far ignored in simulations of materials for photovoltaic and thermophotovoltaic applications, are shown to be of relevance for both conduction (TM Mode) and valence-band based (TE Mode) configurations.

OCIS codes: 040.2235, 040.5350, 230.5590, 350.6050

1. Introduction

Materials for intersubband (ISB) optics are leading to a plethora of significant advances based on the generation and detection of mid infrared and THz radiation[1]. In this paper, we focus on an application of those materials and structures that have been so far mostly overlooked: increasing the efficiency of photovoltaic solar cells, which is one of the current challenges for science and technology [2]. In conventional single-energy-gap photovoltaic devices, only photons with energy close to the semiconductor bandgap are effectively absorbed and converted into current. The semiconductor is transparent for photons with energy smaller than the bandgap. One solution for this problem is to introduce intermediate bands (IBs) in the gap. However, IB designs suffers from two contradictory requirements: (a) the IB should exhibit a finite energy width so that it can be partially occupied to facilitate simultaneous excitation from the IB to the conduction band and from the valence band to the IB. (b) the IB should be as narrow as possible to reduce carrier transport through the miniband [3]. Furthermore even those cannot usually absorb far infrared photons. In contrast, intersubband (ISB) - based thermophotovoltaic (TPV) devices are not limited by the bandgap and can absorb photons very far in the infrared without suffering from the issues (a,b). As a matter of fact, ISB transitions already form the basis of well established devices such as quantum cascade lasers [4] and quantum well infrared photodetectors (QWIPs) [5]. TPVs can enhance the efficiency of existing thermal plants and recover energy lost in a number of different engines, including automobiles. They can be customized for specific applications and tuned to different source temperatures. Like thermoelectric devices, TPVs can generate electricity from different types of heat sources including combustion processes, radioactive isotopes, sun light, geothermal heat as well as nuclear and conventional reactors [6].

The present state-of-the-art in TPV energy conversion from a thermal source at a temperature of 1300 K is about 0.8 W/cm2, obtained with a 0.6-eV bandgap energy InGaAs interband photodetector grown lattice mismatched on InP with an InPAs buffer and the simulations in Ref. [7] indicate that at the same temperature an ISB TPV depicted can potentially generate 1.4W/cm2. We can therefore conclude that the multiple-junction ISB device concept has the potential to provide a substantial improvement over existing technologies.

Note that one difficulty for conventional conduction-band based structures, as in Ref. [7],

is how to absorb photons normal to the surface efficiently, since for usual bandstructures only TM mode absorption is possible for conduction subbands. This is the same problem of QWIPs. One solution is to use a grating or photonic band gap coupler, but this can impart a loss on the broad spectral coverage.

Before proceeding further it is useful to summarize unique features of this study not found previously in the literature.

(i) A possibly more efficient solution for energy extraction in the far infrared is investigated: intervalence-band based designs that lead to TE mode absorption and can directly absorb photons normal to the surface.

(ii) Furthermore, many body effects due to the electron-electron interaction have a proven relevance in semiconductor lasers in both interband [8, 9, 10] and intersubband optics [11, 12, 13, 14, 15, 16, 17], but have so far been ignored in studies of photo and thermo photovoltaics. They are analyzed here, their relevance is clear and may be particularly important for hot carrier architectures [18] where a large density of nonequilibrium carriers can be created. They are shown to be important for structures operating under both TE and TM incidence.

There are as yet no TE mode valence-band-based TPVs. The experimental evidence of TE valence band based electroluminescence in semiconductor heterostructures [19], make clear that such devices are feasible. The theoretical analysis presented here is thus timely to stimulate further experimental efforts in this promising field.

2. Numerical Results and Discussion

The ISB optical response of the semiconductor material is treated fully quantum mechanically by means of our NGF approach [13, 14]. The photocurrent generation spectrum collected by each period (n) with length d_n, which is here simply the Quantum Well width, is given by [20]

$$J_n(\omega) = q \int_{z_n}^{z_n+d_n} G_n(\omega, z) dz, \tag{1}$$

where the generation rate reads

$$G_n(\omega, z) = \alpha_n(\omega) F(\omega) [1 - R(\omega)] e^{-\alpha_n(\omega) d_n}. \tag{2}$$

In Eq. (2) $R(\omega)$, is the surface reflection coefficient, $F(\omega)$ is the photon flux incident on the sample surface and z_n is the position of the QW along the device's growth direction. The absorption coefficient $\alpha_n(\omega)$ stems from the imaginary part of the susceptibility $\chi(\omega)$,

$$\alpha_n(\omega) = \frac{4\pi\omega}{cn_b} Im\{\chi(\omega)\}, \;\; \chi(\omega) = 2 \sum_{\mu\neq\nu,\vec{k}} \wp_{\mu\nu}\, \chi_{\nu,\mu}(k,\omega). \tag{3}$$

Here n_b denotes the background refractive index, c is the speed of light, $\wp_{\nu\mu}$=$ed_{\nu\mu}$ is the transition dipole moment between the subbands ν and μ, The first step is the solution of the 8 band $\mathbf{k}\cdot\mathbf{p}$ Hamiltonian. The Green's functions and self-energies are expanded using eigenstates and eigenvalues of this Hamiltonian. Since the electrons are assumed to be in equilibrium when they are promoted to a higher energy subband by absorption of a photon, the full NGF scheme is simplified and reduces to the self-consistent evaluation of chemical potentials and self-energy matrix elements which lead to subband energy renormalisation, dephasing constants and occupation functions. Finally, the susceptibility function that leads to the absorption is given by the solution of the integro-differential equation for $\chi_{\nu\mu}(k,\omega)$ obtained from the carriers Green's function in linear response,

$$\left[\hbar\omega - e_{\nu\mu}(k) + i\Gamma_{\nu\mu}\right]\chi_{\nu\mu}(k,\omega) - \delta n_{\nu\mu k} \sum_{\mathbf{k}'\neq\mathbf{k}} \chi_{\nu\mu}(k',\omega)\tilde{V}^{\nu\mu}_{\mathbf{k}-\mathbf{k}'} = \wp_{\nu\mu}(k)\delta n_{\nu\mu k}\,, \tag{4}$$

where $\delta n_{\nu\mu k}$ =$n_\nu(k)$-$n_\mu(k)$ denotes the nonequilibrium population difference between subbands ν and μ. Further details of the renormalised energies $e_{\nu\mu}$, electron-electron scattering broadening $\Gamma_{\nu\mu}$ and the Coulomb matrix elements $\tilde{V}^{\nu\mu}_{\mathbf{k}-\mathbf{k}'}$ are given in Ref. 13.

Note that the intersubband relaxation is different for conduction and valence bands. Forthcoming research will include all relevant scattering mechanisms beyond the electron-electron scattering, along the lines of Ref. [16] and extending that research to the case of arbitrary dispersion relations considered here. The occupations will be computed accordingly through the full solution of the corresponding Dyson equations. Depending on the design and the transitions exploited, the interplay between the different scattering mechanisms can lead to faster relaxation in the valence bands as expected in simple designs. This may reduce the TE mode TPV efficiency and will be investigated in detail.

The numerical results presented next are for a single junction section composed of either a 5 nm or a 10 nm $GaAs-Al_{0.3}Ga_{0.7}As$ quantum well. In all curves the valence band (for TE polarization) and conduction band (for TM polarization) electrons available due to doping are initially thermalized at 300K. Figures 1.a and 1.b compare and contrast the Photocurrent

Generation Spectra with TE polarization with and without many body corrections at the same level as in Ref. [13]. There is a clear difference between free carrier (dashed curves) and manybody (solid lines) calculations, highlighting the need of combining ab initio and/or $k \cdot p$ electronic structure with NGF or density matrix methods to include manybody effects for realistic predictions of PV and TPV materials and devices. Extra structure develops notably on the low energy side of the TE mode due to a combination of band nonparabolicity and manybody effects as the carrier density increases. Those effects can be engineered to increase the absorption in certain spectral regions and are thus an extra tool to improve TPV efficiencies.

Figures 1.c and 1.d show the evolution of the Photocurrent Generation Spectra at the TE mode for different thermal photon source temperatures. The incident photon flux shifts to higher energies with increasing thermal source temperatures leading to a relative increase in the peaks in the higher energy side.

The photocurrent spectra is thus more complex than just the absorption shown in Ref. [13] and customized structures for different types of thermal sources should be designed considering all those effects together. Figure 2 shows corresponding results for the TM mode. Manybody corrections lead to the redistribution of oscillator strength and higher contrast is quite noticeable in the TM mode. As the thermal source temperature increases, the spectra are further modified similarly to what happens in the TE mode.

Note that all TM mode results here are for the maximum possible effective transition dipole moment and all practical results would be smaller. The actual oscillator strengths of the transitions are reduced by the unavoidable nonzero incidence angle. Thus losses appear due to projection plus further prism/coupler losses that can reduce the TM photocurrent by an order of magnitude. This further favours the study of valence band based TE mode in the far infrared for structures intended to extract photons in that range. Thus, Fig. 3 compares and contrasts the far infrared range performance of the quantum well absorbers for perpendicular incidence in the TE mode and maximum incidence TM mode.

Regardless of a much larger transition dipole in the mid infrared range for the TM case, the far infrared is dominated by the TE polarization. Lower photon source temperatures further favour the TE case by enhancing the photocurrent in the lower energy side.

In summary, this study demonstrates that inter-valence band absorption structures may lead to devices that can potentially convert thermal photons in the far infrared efficiently

into current. This is a range that remains to be further exploited. Absorption due to intervalence band transitions allows simple perpendicular incidence in the TE mode without the need of prisms or other couplers, in contrast to interconduction-band-based TPVs, thus simplifying the designs and avoiding corresponding optical losses. Furthermore, the analysis demonstrates the relevance of many body effects, which are now routinely considered in laser and optoelectronic device simulators, but have been essentially overlooked for photo and thermophotovoltaic simulation and design considerations. Those effects should be considered in both intersubband and interband cases for all polarizations. I hope that this paper will stimulate further experimental studies to improve the carrier collection in the p-doped case that may lead to a new generation of valence-band-based TPV devices. Note that this study can be extended to other materials like Si-SiGe that so far have performed poorly in light emitting applications but can potentially become very efficient for current generation based on far infrared photons.

References

1. B. Ferguson and X.-C. Zhang, "Materials for Terahertz Science and Technology," Nature Materials **1**, 26-33 (2002).
2. A. Feltrin and A. Freundlich, "Material Considerations for Terawatt. Level Deployment of Photovoltaics," Renewable Energy, **33**, 180-185 (2008).
3. S. Tomić, "Intermediate-band solar cells: Influence of band formation on dynamical processes in InAs/GaAs quantum dot arrays," Phys. Rev. B **82**, 195321-1 - 195321-15 2010).
4. J. Faist, F. Capasso, D.L. Sivco, C. Sirtori, A.L. Hutchinson, A.Y. Cho, Science Cho, "Quantum Cascade Laser," **264**, 553-556 (1994).
5. M. Graf, G. Scalari, D. Hofstetter, J. Faist, H. Beere, E. Linfield, D. Ritchie, and G. Davies, "Terahertz range quantum well infrared photodetector," Appl. Phys. Lett. **84**, 475-477 (2004).
6. C. Goupil, "Thermodynamics of the thermoelectric potential," J. Appl. Phys. **106**, 104907-1 - 104907-4 (2009).
7. J. Yin and R. Paiella, "Multiple-junction quantum cascade photodetectors for thermophotovoltaic energy conversion," Optics Express **18**, 1618-1629 (2010).
8. M.F. Pereira Jr, R. Binder and S.W. Koch,"Theory of nonlinear optical absorption in

coupled-band quantum wells with many-body effects," Appl. Phys. Lett. **64**, 279-281 (1994).

9. M.F. Pereira Jr and K. Hennerberger, " Gain Mechanisms and Lasing in II-VI Compounds", phys. stat. sol. (b) 202, 751 (1997).
10. M.F. Pereira Jr and K. Hennerberger, "Microscopic Theory for the Optical Properties of Coulomb-Correlated Semiconductors" , phys. stat. sol. (b) 206, 477 (1998).
11. G. Scalari, S. Blaser, J. Faist, H. Beere, E. Linfield, D. Ritchie and G. Davies, "Terahertz Emission from Quantum Cascade Lasers in the Quantum Hall Regime: Evidence for Many Body Resonances and Localization Effects," Phys. Rev. Lett. **93**, 237403-1 - 237403-4 (2004).
12. J. Li and C.Z. Ning, Phys. Rev. B "Effects of electron-electron and electron-phonon scatterings on the linewidths of intersubband transitions in a quantum well," **70** 125309-1 - 125309-8 (2004).
13. M.F. Pereira Jr. and H. Wenzel, "Interplay of Coulomb and nonparabolicity effects in the intersubband absorption of electrons and holes in quantum wells," Phys. Rev. B **70**, 205331-1 - 205331-8(2004).
14. R. Nelander, A. Wacker, M.F. Pereira Jr., D.G. Revin, M.R. Soulby, L.R. Wilson, J.W. Cockburn, A.B. Krysa, J.S. Roberts and R.J. Airey, "Fingerprints of spatial charge transfer in quantum cascade lasers," Journ. Appl. Phys. **102** 113104-1 - 113104-5 (2007).
15. M.F. Pereira Jr, "Intersubband antipolaritons: Microscopic approach, "Phys. Rev. B **75** 195301-1 - 195301-5 (2007).
16. T. Schmielau and M.F.Pereira Jr, "Nonequilibrium many body theory for quantum transport in terahertz quantum cascade lasers," Appl. Phys. Lett. **95** 231111-1 - 231111-3 (2009).
17. Thi Uyen-Khanh Dang, Carsten Weber, Martin Richter and Andreas Knorr, "Influence of Coulomb correlations on the quantum well intersubband absorption at low temperatures," Phys. Rev. B **82**, 045305-1 - 045305-5 (2010).
18. A. Le Bris and J.F. Guillemoles, " Hot carrier solar cells: Achievable efficiency accounting for heat losses in the absorber and through contacts," Appl. Phys. Lett. **97**, 113506-1 - 113506-3 (2010).
19. S. A. Lynch, D. J. Paul, P. Townsend, G. Matmon, Z. Suet, R. W. Kelsall, Z. Ikonic, P.

Harrison, J. Zhang, D. J. Norris, A. G. Cullis, C. R. Pidgeon, P. Murzyn, B. Murdin, M. Bain, H. S. Gamble, M. Zhao, and W.-X. Ni, "Toward Silicon-Based Lasers for Terahertz Sources, " IEEE J. Select. Topics Quantum Electron **12**, 1570-1578 (2006).

20. V. Aroutiounian, S. Petrosyan, A. Khachatryan andK. Touryan,"Quantum Dot Solar Cells," Journ. Appl. Phys. **89**, 2268-2271 (2001).

Figure Captions

Figure 1: (Colour online) Photocurrent generation spectra of Eq. 1. with (solid) and without manybody effects (dashed) for one section of a possible ISB device with 5 nm (a,c) and 10 nm (b,d) QW active regions with TE polarization. From bottom in to top in (a,b) the valence band carrier density is increased by N=1 and 3 $\times$ 10^{12} cm^{-2}. The thermal photon source temperature is T=1000 K. From bottom to top in (c,d) the thermal source carrier temperature is increased from T=500K to T=1000 K. The valence band carrier density is N= 3 $\times$ 10^{12}.

Figure 2: (Colour online) Photocurrent generation spectra of Eq. 1. with (solid) and without manybody effects (dashed) for one section of a possible ISB device with 5 nm (a,c) and 10 nm (b,d) QW active regions with TM polarization. From bottom in to top in (a,b) the conduction band carrier density is increased by N=1 and 3 $\times$ 10^{12} cm^{-2}. The thermal photon source temperature is T=1000 K. From bottom to top in (c,d) the thermal source carrier temperature is increased from T=500K to T=1000 K. The conduction band carrier density is N= 3 $\times$ 10^{12}.

Figure 3: (Colour online) Comparison of TE (solid-black) vs TM mode at a maximum angle of incidence (dashed-green) photocurrent generation spectra for the QWs of Figs. 1 and 2. The doping density is $N = 3 \times 10^{12}$ cm^{-2} thermalized at 300 K. The QW well widths are 5 nm for (a,c) and 10 nm for (b,d). The thermal source temperatures are 500 K for (a,b) and 1000 K for (c,d). All panels have the same relative scale to allow a direct comparison. Note that actual TM mode absorption would be smaller due to the angles of incidence and prism/coupler losses. This means that the TM mode generation spectra would be even smaller then shown here, further supporting a study of TE valence band-based materials and designs for the far infrared.

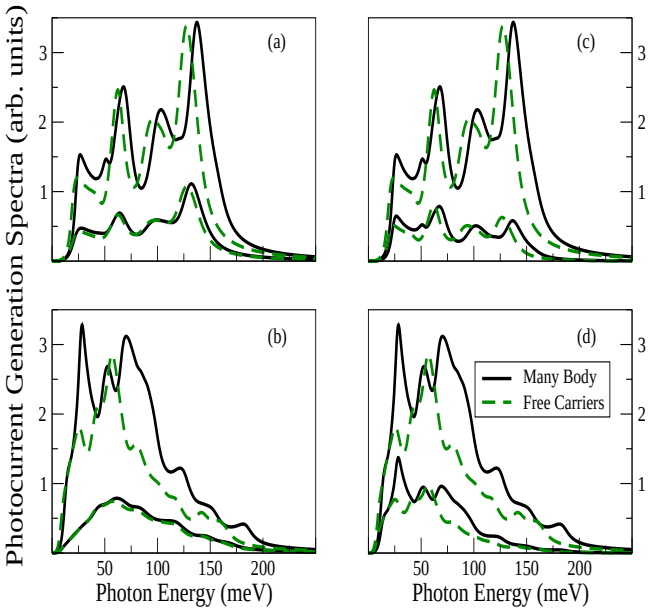

Fig. 1. (Colour online) Photocurrent generation spectra of Eq. 1. with (solid) and without manybody effects (dashed) for one section of a possible ISB device with 5 nm (a,c) and 10 nm (b,d) QW active regions with TE polarization. From bottom in to top in (a,b) the valence band carrier density is increased by N=1 and 3 $\times$ 10^{12} cm^{-2}. The thermal photon source temperature is T=1000 K. From bottom to top in (c,d) the thermal source carrier temperature is increased from T=500K to T=1000 K. The valence band carrier density is N= 3 $\times$ 10^{12}.

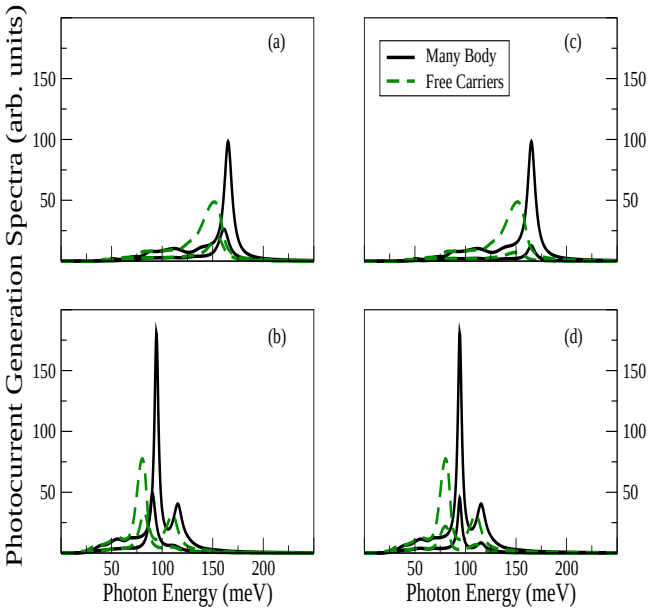

Fig. 2. (Colour online) Photocurrent generation spectra of Eq. 1. with (solid) and without manybody effects (dashed) for one section of a possible ISB device with 5 nm (a,c) and 10 nm (b,d) QW active regions with TM polarization. From bottom in to top in (a,b) the conduction band carrier density is increased by N=1 and 3 $\times$ 10^{12} cm^{-2}. The thermal photon source temperature is T=1000 K. From bottom to top in (c,d) the thermal source carrier temperature is increased from T=500K to T=1000 K. The conduction band carrier density is N= 3 $\times$ 10^{12}.

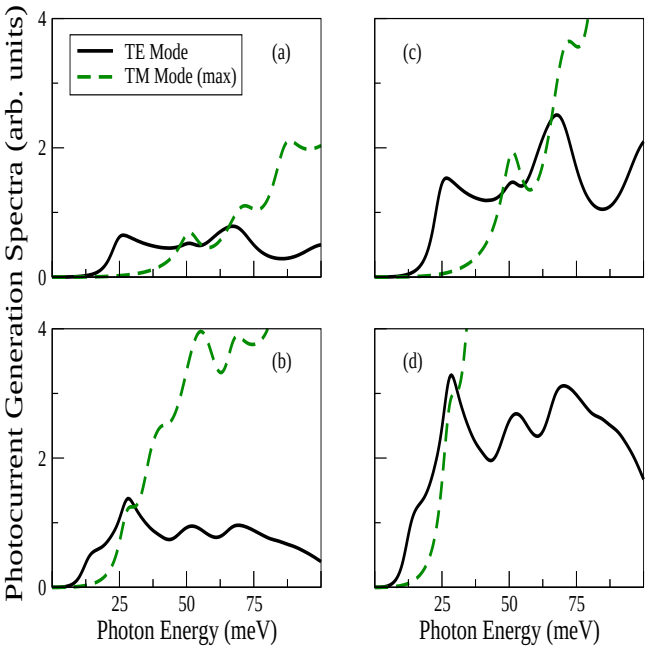

Fig. 3. (Colour online) Comparison of TE (solid-black) vs TM mode at a maximum angle of incidence (dashed-green) photocurrent generation spectra for the QWs of Figs. 1 and 2. The doping density is $N = 3 \times 10^{12}\ cm^{-2}$ thermalized at 300 K. The QW well widths are 5 nm for (a,c) and 10 nm for (b,d). The thermal source temperatures are 500 K for (a,b) and 1000 K for (c,d). All panels have the same relative scale to allow a direct comparison. Note that actual TM mode absorption would be smaller due to the angles of incidence and prism/coupler losses. This means that the TM mode generation spectra would be even smaller then shown here, further supporting a study of TE valence band-based materials and designs for the far infrared.